6th European Conference on Computational Mechanics (ECCM 6)
7th European Conference on Computational Fluid Dynamics (ECFD 7)
1115 June 2018, Glasgow, UK

AERODYNAMIC OPTIMIZATION OF A PARAMETRIZED ENGINE PYLON ON A MISSION PATH USING THE ADJOINT METHOD

Damien Guénot[1,2], François Gallard[1], Joël Brézillon[3,1] and Yann Mérillac[2]

[1] IRT Saint Exupéry
B 612 - 3 Rue Tarfaya - CS 34436 - 31405 Toulouse CEDEX 4 (France)
email : francois.gallard@irt-saintexupery.com

[2] Altran Technologies
4 Avenue Didier Daurat - 31700 Blagnac (France)
email : {damien.guenot,yann.merillac}@altran.com

[3] Airbus Operations SAS
316 Route de Bayonne - 31060 Toulouse (France)
email : joel.brezillon@airbus.com

Key words: CAD parametrization, Engine pylon, MDO, CFD, Adjoint

Abstract. In the frame of the MDA-MDO project at IRT Saint-Exupéry, an aircraft engine pylon multidisciplinary optimization is performed. The MDO process uses industrial tools for aerodynamic, structural and overall aircraft design disciplinary optimization. A bi-level MDO formulation is selected, enabling the reuse of the disciplinary optimization software while ensuring the convergence to a true MDO optimum. This study focuses on the adjoint-based aerodynamic multi-point optimization part of the MDO study. Thereby, a fully parametrized pylon CAD has been developed. More than 400 variables are required to obtain an accurate shape representation of the pylon and to take into account for various design constraints such as system integration or slats deployment, while giving enough degrees of freedom to optimize the complete 3D pylon shape. A particular challenge of the engine integration test case is the computation of many complex intersections : wing with pylon, pylon with engine nacelle and pylon with fan exit. These intersections must be deformed according to the new pylon shape at each optimization iteration, while keeping the exact shape of the nacelle and wing constant. The parametrization and mesh deformation are therefore largely impacted by these intersections. The overall process must be differentiated to benefit from the discrete adjoint of the CFD solver.

First, an optimization in cruise condition ($C_L = 0.47 - Mach = 0.83$) is performed. Then, multiple operating conditions are added in the optimization formulation, in order to get a robust design. Finally, a trade off is performed with a design of experiments study on the engine position, where a local optimization is performed for each of them. These results demonstrate that the capability is able to handle the 3D complex pylon geometry with its full intersections with the nacelle and the wing.

1 INTRODUCTION

1.1 Presentation of the XRF1 pylon MDO test case

The purpose of the MDA-MDO project of IRT Saint-Exupéry [6] is to optimize an aircraft pylon with high-fidelity methods, in consistency with the global aircraft level, at a lower level of fidelity. A bi-level formulation has been developed for the project needs, as this family of formulations is well suited for a direct industrial use.
The Airbus XRF-1 transport aircraft configuration is used as the reference geometry. The XRF-1 is a generic research configuration of a wide-body aircraft delivered by Airbus to its partners in order to ease the development of MDO capabilities. To this aim, a shape is provided along with additional information such as load cases and a finite element model.

1.2 Objective of the present study

As mentioned earlier, the bi-level MDO formulation selected for the present study has the benefit of using directly disciplinary optimization processes.
The present study is about the aerodynamic optimization of the pylon external shape, within the MDO process. This industrial optimization suite has already been successfully applied to the optimization of the XRF-1 wing [3].

The main steps of the study are :

- Build a parametrized pylon CAD with both global and local design variables,
- Generate CAD deformations from the parametric CAD, accounting for intersections with the fixed wing and nacelle CADs,
- Validate the CAD deformation process on CFD computation, through mesh deformation,
- Validate the optimization process on a single operation condition,
- Validate the optimization process for multiple operating conditions.

2 AERODYNAMIC PARAMETRIZATION OF THE PYLON

2.1 PADGE (Parametric And Differentiated Geometrical Engine)

PADGE is an Airbus in-house CAD engine used by IRT for aerodynamic optimization. Its main features are :

- Fully parametric, ie the whole model can be automatically updated when design variables are changed.
- Based on NURBS [8], so compatible with CAD formats.
- Full differentiation: the total derivative of any point, line or surface in the model with respect to the design variables can be computed. This is mandatory to allow an efficient use of gradient-based optimization algorithms.
- Ensure shape smoothness, quality, and geometrical constraints thanks to a wide range of interpolation and surfacing methods.

2.2 Parametrization of the pylon external shape

In the present study, the only global design variable considered is the engine relative displacement on the x axis. Additional global variables will be added in the future, such as the engine position on the z axis, or the pylon widths. Attachment points between the wing and the pylon are fixed, so when moving the engine forward, some surfaces have to be able to be stretched whereas some others are fixed.

In order to ensure relevant optimization, design variables have to be representative of user needs in term of design activities or physical analysis. It is also advantageous to express most of the user constraints as bounds on the design variables rather than non-linear constraints as they typically slow the optimization process or may deal with feasibility issues. Considering CAD based design, a parametrization based on nodes position is meaningless for a designer who is used to think in terms of curvature radius, camber or slope angles. A last important requirement deals with the external constraints management : in a multi-disciplinary approach, parametrization must be able to handle constraints from other disciplines such as slat deployment or system pipes.

The parametrization setup of the pylon follows a three steps process:

- Build a generic template of the pylon based on NURBS and Coons patches with deformation capabilities based on physical variables : points, curves and surfaces have variables controlling their position, curvature and tangent angles.
- Match these design variables to fit to the template with baseline shape. This matching process is a minimization problem solved by a non-linear least-square method.
- Freeze a subset of these variables and set the bound of the remaining ones as design variables for the optimization problem.

Considering all these requirements, more than 1100 variables are needed to obtain a parametrized shape of the pylon that accurately fits the baseline XRF1 geometry. This number is relatively high because the pylon is a complex and fully 3D, non-symmetrical shape. Taking into account for the geometrical constraints, the final parametrization has about 400 free design variables provided to the optimizer.

Intersections computation

One of the challenging aspect of the pylon parametrization is the computation of all intersections of pylon with wing, nacelle and fan outlet, and then the morphing of the surface mesh according to these intersections. A simple surfaces intersection is an intersection between two single NURBS patches. However, the different components are not made of single CAD surfaces but sets of surfaces, called the families of surfaces. Managing intersections through families is more convenient as it handles automatically creation of intersection between the surfaces of the two families. The families of surfaces are intersected together to generate the surface mesh morphing. This allows the intersections and morphing of complete aircraft components together, such as the pylon with the wing, the pylon with the nacelle and the fan outlet (triple intersection). Final result of intersections computation is shown on Figure 1.

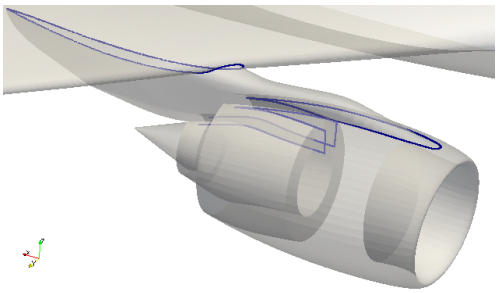

Figure 1: Intersections of wing with pylon, pylon with engine and pylon with fan exit

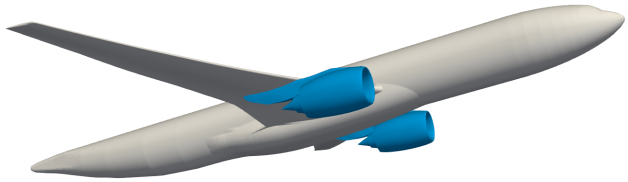

Figure 2: Simplified XRF1 CAD model used in aerodynamic process

3 AERODYNAMIC OPTIMIZATION PROCESS

3.1 Presentation of the aerodynamic shape optimization process

The optimization problem setup and the connection with the gradient based optimizer are managed by GEMS (Generic Engine for MDO Scenarios) [5], a tool developed at IRT. The aerodynamic simulation process, based on files exchanges on the HPC is managed with WORMS (WORkflow Management System), an Airbus workflow manager [3].

In order to propagate the surface deformation field computed by PADGE into the volume, an integral formulation method is used [7]. For the computation of the surface grid sensitivity, a reverse mode by analytical differentiation, is available.

The pressure drag is considered as objective function since it accounts for most of the variations of the total drag of the XRF-1 configuration, as shown for baseline configuration on Figure 4. The extension to the use of the cash operating cost as objective function of the MDO study, as mentioned in the introduction, can be extended from the multi-point condition optimizations by an adequate computation of the weights, as explained in [3].

3.2 Mesh deformation process

A simplified geometry of the XRF1-1 model is used for the aerodynamic process and is shown on Figure 2 : HTP (Horizontal Tail Plane), VTP (Vertical Tail Plane) and FTF (Flap Track Fairing) are removed. This simplification allows to get a smaller mesh size while catching all physical aspects dealing with pylon's influence. A multi-block structured mesh mesh dedicated to this study has been build with about 7.10^6 nodes.

In the present MDO study, the engine position, controlled by the dX variables, varies in the range $[-300\text{ mm}, 100\text{ mm}]$ relatively to the reference position. A surface displacement field $\Delta x\vec{y}z$ generated by the CAD parametrization is shown on Figure 3. The Aft Pylon Fairing (APF) and its nearest zone of pylon have moved by dX (in blue for $dX = -300$ mm and in red for $dX = -100$ mm), while in the neighborhood of the wing, deformations are small (light red) : this is due to the fixed attachment points of the pylon on the wing. Between the wing and the APF, as well as on the front pylon nose, buffer areas allow smooth deformations between regions that are almost fixed and regions that have to move with the engine, such as the APF.

(a) $dX = -300$ mm (b) $dX = 100$ mm

Figure 3: Magnitude of deformation field on the surface mesh

3.3 CFD Solver

The numerical computation of the flow is performed by the *elsA*-ONERA CFD solver [1], which solves the compressible 3D RANS equations. Turbulence is solved using the Spalart-Allmaras model based on a single transport equation for the eddy viscosity-like variable $\tilde{\nu}$. A discrete adjoint solver is used to compute the derivatives of the drag with respect to the volume mesh and all of the methods in the flow solver are differentiated by hand. The turbulent eddy viscosity and thermal conductivity are assumed constant during the differentiation.

3.4 Validation

Optimization mesh

In order to obtain the optimization result within a turnaround time compatible with industrial design constraints, a light optimization mesh of 6.6 10^6 nodes is used as a compromise. The challenge is, with such a light mesh, to accurately capture the flow features around the engine installation, and the exact drag variations brought by the optimization. A much finer mesh, with 120 10^6 nodes, is used to validate the performance gains obtained on the optimization mesh. This second mesh is finer in terms of discretization. It has also a more accurate geometrical representation of the aircraft with additional components: the FTF, the HTP and VTP.

On Figure 5, the contours represent the pressure coefficient C_p. On this colormap, compression to expansion are colored from blue to red. All relevant features, such as expansion/compression on the inner/outer part near the engine outlet, compression at the stagnation point around the inner wing junction can be found on the solutions obtained from the two meshes. On bottom view, the influence of the FTF on the pressure coefficient is visible but the overall flow features around the pylon are similar.

The last views compare the friction vector modulus on Figure 6 : once again, both meshes are able to capture the separation that occurs on the rear part of the pylon and their extent are matching, while their amplitude is significantly different close to the wing trailing edge. By observing the friction lines, this can be explained because the FTF induce a significant deviation of the flow in the span-wise direction, which reduces the adverse pressure gradient in this area and therefore the flow separation that occurs at the trailing edge of the pylon.

This qualitative comparison confirms the proper use of lighter mesh in the optimization context concerning the qualitative aspects of the flow. The exact drag variations values computed on the light mesh shall be checked on the finer mesh since the pressure values are similar but not exactely equal on the two meshes.

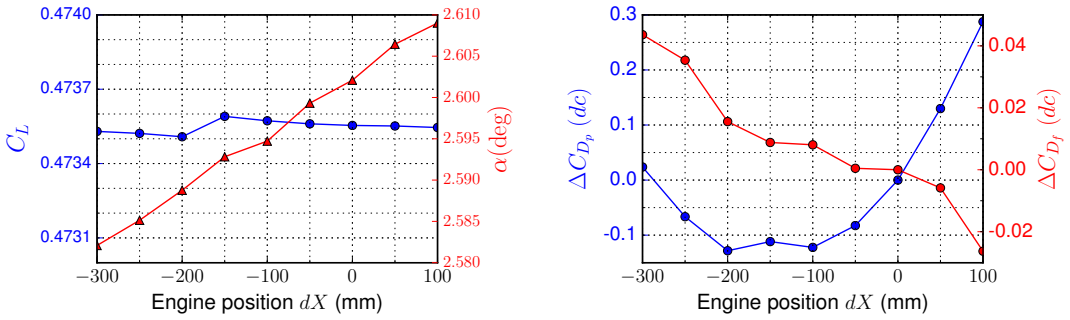

Figure 4: Influence of engine position on lift and drag coefficients (pressure and friction) on baseline configurations

Volume mesh deformation with CFD computations

The deformation field in the volume mesh is extrapolated from the surface deformation field prescribed by the parametrization, using an inverse distance interpolation method [7]. Figure 4 shows the influence of the engine position on the global force coefficients : the left figure displays lift coefficient values as well as corresponding angle of attack for 9 engine positions. The right figure shows the pressure and friction drag coefficient resulting of a near field analysis. All drag coefficients are given compared to the baseline geometry.
At first order, moving engine towards the aircraft nose should increase the pylon wet surface, which logically leads to a small increase in friction drag. But, as the relative variation is small compared to pylon size, this increase is almost negligible.

These first computations validate the aerodynamic process, from CAD deformation to post-processing.

4 DEMONSTRATIONS

4.1 Single point optimizations

The CFD computations on the deformed geometries show that the local deformations have a negligible influence on the lift. This can be explained because the pylon is a non-lifting surface. Hence, the CFD computations are performed at a fixed angle of attack in the optimization loop. This avoids either a target lift resolution in the CFD solver or a lift constraint in the optimization problem, which both cost an adjoint computation for the lift coefficient. Moreover, to reduce computation time, the direct and adjoint computations are warm started from the baseline solutions. The turnaround times for the optimization process are summarized in Figure 7. The L-BFGS-B optimization algorithm is used to drive the optimization process. It is a gradient based algorithm for bound constrained problems, available through GEMS interface [5].

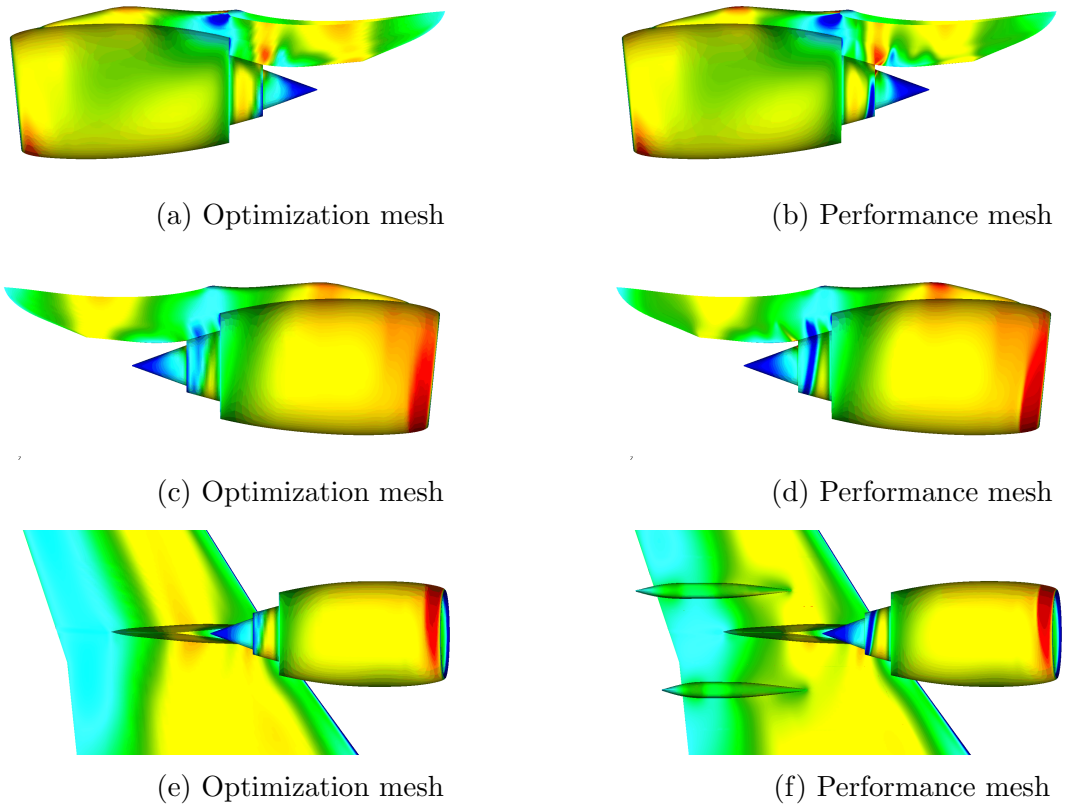

(a) Optimization mesh (b) Performance mesh

(c) Optimization mesh (d) Performance mesh

(e) Optimization mesh (f) Performance mesh

Figure 5: Pressure coefficient for optimization mesh and performance mesh on baseline geometry

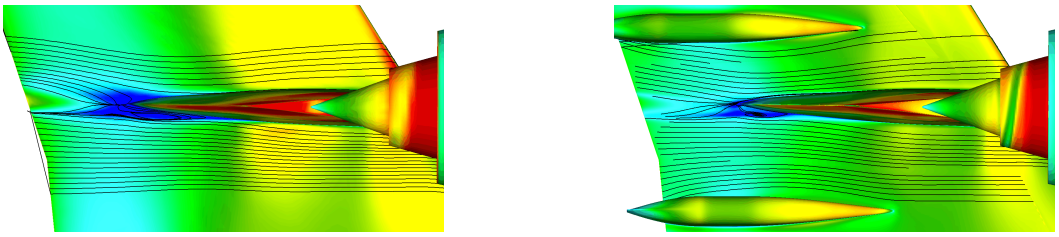

(a) Optimization mesh (b) Performance mesh

Figure 6: Friction coefficient modulus and friction lines for optimization mesh and performance mesh on baseline geometry

Convergence histories and optimizations results

The flight condition used in the single point optimizations are the followings : $Mach = 0.83$, $Re = 49.9\ 10^6$, $\alpha = 2.6$. For all results presented hereafter, the reference value used in plots or tables is the value for the baseline configuration with $dX = 0$ mm. Table 8 shows the convergence history for reference engine position. The pressure drag is reduced of 0.8 dc (drag count) after 12 steps (tunraround time of 36 hours). The optimal solution provides an improvement of 1.2 dc on total drag after 27 iterations (tunraround time of

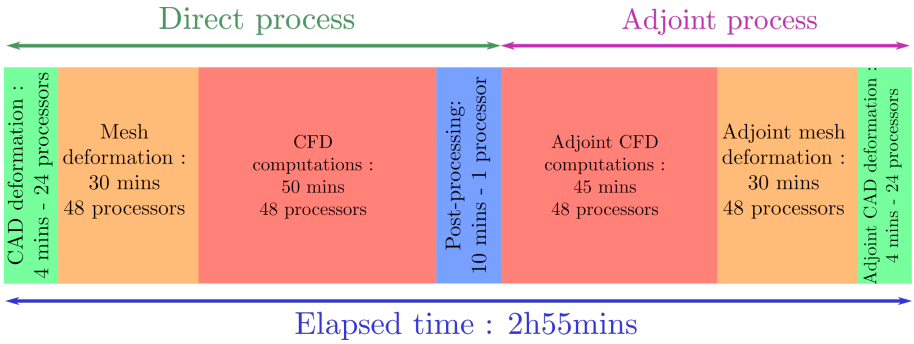

Figure 7: Distribution of elapsed time for one optimization iteration

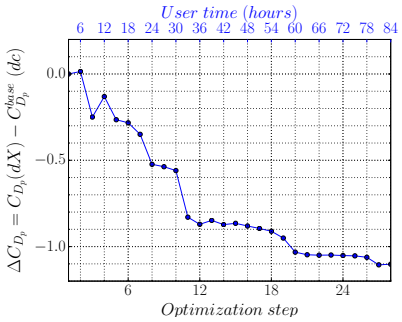

Figure 8: Convergence history of the single point optimization for $dX = 0$ mm

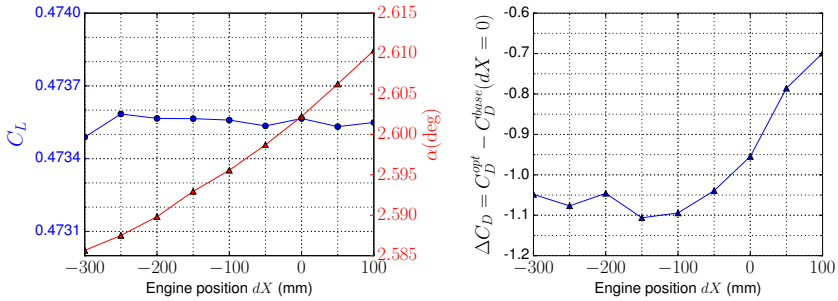

Figure 9: Optimum performance of the single point optimizations for various engine positions at $C_L = 0.4735$ - $M = 0.83$ w.r.t to baseline geometry

81 hours).

Table 9 shows the final results for nine engine positions : the optimizer manages to decrease the total drag between 0.7 and 1.1 *dc* with respect to the baseline geometry. Compared to what can be achieved with the optimization on a wing [3], this gain is small but the contribution of a pylon to the total drag is small. For aircraft designers, this global drag decrease is however significant when considering a pylon.

Influence of optimization on surface flow fields

Comparing pressure coefficient for the optimal geometry on Figure 10 to the baseline geometry on Figure 5, optimization process leads to several changes (black ellipses):

- On the pylon nose, upstream displacement leads to a smoother expansion of the flow compared to baseline geometry. The expansion spot on the upper bump of the baseline geometry (Figure 10a and Figure 10c) almost disappeared. Moreover, the expansion is smoothed on the slope going from the nacelle to the upper bump while on the baseline geometry, there are some expansion and compression areas.
- On the rear sides, as the pylon is fattened before the trailing edge, the expansion is less important. But this also leads to an increase in pressure gradients before the trailing edge. This behaviour can be seen on both sides of the pylon, and is stronger on the inner part.

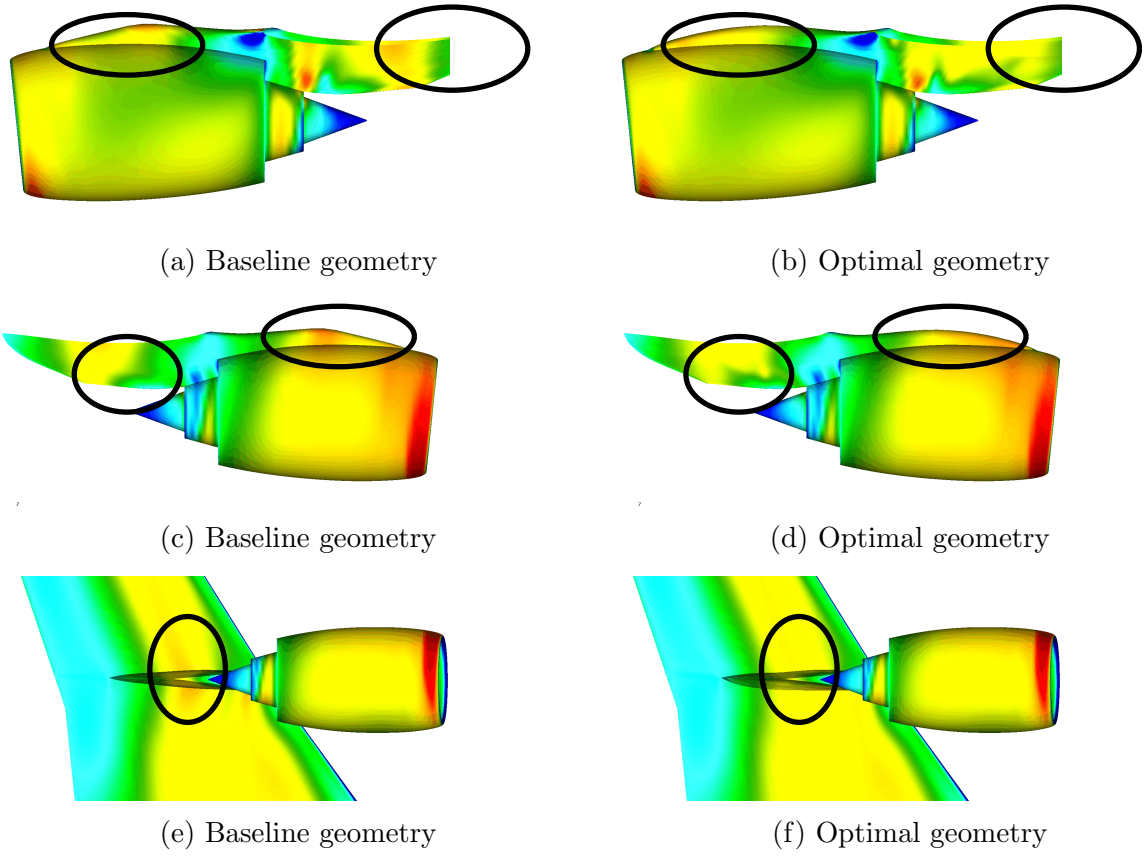

(a) Baseline geometry

(b) Optimal geometry

(c) Baseline geometry

(d) Optimal geometry

(e) Baseline geometry

(f) Optimal geometry

Figure 10: Pressure coefficient for optimal and baseline geometry for reference engine position

(a) Baseline geometry

(b) Optimal geometry

Figure 11: Friction coefficient modulus and friction lines for optimal and baseline geometry for reference engine position

Figure 11 shows that optimization did not manage to fully remove flow separation at the rear part of the pylon. This may be due to the bounds on the design variables, restricting the design space, or to the noise due to the frozen turbulence hypothesis in the adjoint solver. Flow separations largely impact the velocity gradients so the turbulence solution, so having a frozen turbulence hypothesis may be too restrictive since it is known that it can significantly affect the optimization [2].

This first achievement shows that the shape parametrization is well suited for controlling the main flow features around the pylon. Besides, the optimal shape is not wavy,

which would make it unsuitable for manufacturing. The drag improvements are driven by physical phenomena that can be explained.

4.2 Multi-point optimization

The final purpose of the project aims at optimizing the XRF1 configuration on a full mission, which requires a multi-point aerodynamic optimization. The Gradient Span Analysis (GSA) method [4] allows the setup of multi-point optimizations by adaptively selecting the minimal number of operating conditions to be included in the optimization problem. Most of the fuel consumption on the XRF1 typical long range mission occurs during cruise ($> 85\%$ of overall block fuel). Hence, a GSA is performed on the cruise conditions with a fixed Mach, and a range of lift coefficient C_L in $[0.3, 0.5]$. As a result, only 3 points are necessary to control the aircraft performance on the continuous C_L interval : $C_L = 0.3$, $C_L = 0.4$ and $C_L = 0.5$.

The objective function is the sum of pressure drag coefficients for all computed conditions. Once again, the local deformations have little influence on the lift coefficient, allowing to have a fixed angle of attack during the optimization process. After iterations (51 hours on 144 CPUs), the pressure drag is decreased by the same order of magnitude for the three operating conditions.

Figure 12 shows the drag polar for the initial lift range. On this figure, the same curve obtained from the previous single point optimization is also plotted. It shows that for the whole lift range, both optimal geometries perform better than the baseline. Comparing single and multi-point optimizations, the single point optimization performs slightly better around its design point but is degraded in off-design conditions by 20% at $C_L = 0.3$. Overall, the multi-point optimum is a much better compromise.

4.3 Trade-off on the engine position

For each engine position, a multi-point optimization is performed on the local variables. This process will be later applied to a MDO trade-off within a bi-level MDO formulation, as explained in the introduction. Figure 13 shows results of pressure drag optimizations with respect to lift coefficient C_L for various engine position displacement dX. As for single point optimization, optimizer always manages to improve drag.

It can be noticed that important variations of drag improvement occur for low C_L values. These variations have the same origin:

- Considering $dX = -50$ mm position, with $C_L \sim 0.32$, and $dX = 50$ mm position, for $C_L = 0.3$, the increase of pressure drag comes from an increase of the separation, already shown on baseline geometry (Figure 6).
- For $C_L = 0.47$, when comparing $dX = -250$ and -300 mm, decrease of optimal performance of Figure 13 can also be explained by an increase of the separation size on the inner part of the wing. This separation also begins earlier on the lower wing.

The best results are obtained for engine displacements of -100 mm and -250 mm which are very close. On the other hand, when $dX > -50$ mm and $dX = -300$ mm, some important flow separations strongly degrade drag decrease compared to baseline geometry.

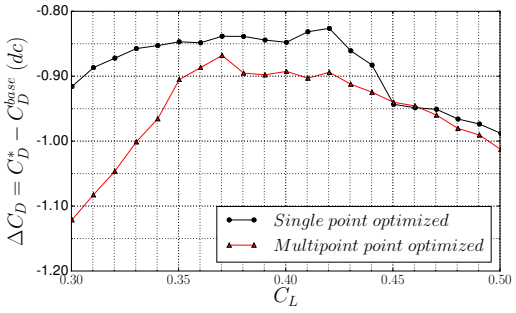

Figure 12: Comparison of drag polars for single point and multi-point optimizations

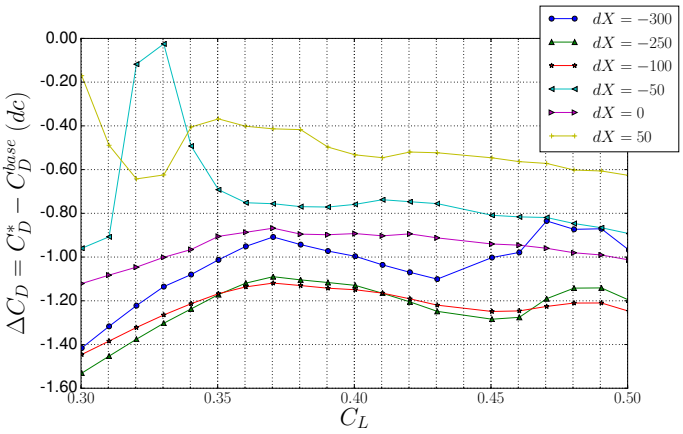

Figure 13: Influence of engine positions dX for multi-point optimizations

Even if no clear trend can be seen, moving engine frontward seems to decrease pressure drag, especally for low lift ($C_L < 0.35$). In this lift range, some drag decreases up to 1.5 dc can be seen, whereas it is of the order of 1.2 dc for higher lift ($C_L > 0.4$). From the different figures shown previously, it seems that rear separation has a major influence of the final result.

5 CONCLUSIONS

An aircraft engine pylon aerodynamic shape optimization was performed in the frame of this study. A key capability realization is the development of a full parametrized pylon shape using a parallel differentiated CAD kernel, which can handle both global and local design variables, and a fast turnaround time (4 minutes on 24 cores). Then, the adjoint-based aerodynamic optimization process was used. A series of single-point and multi-point optimizations, as well as a bi-level trade-off on the engine X position was performed. Overall, the capability is able to handle the complex 3D pylon geometry with its full intersections with the nacelle, the wing and the fan outlet, and perform trade-offs in a MDO context.

The main numerical optimization results can be summarized as:

- A single point optimization around cruise condition ($M = 0.83$, $C_L = 0.473$) improved the total drag by 0.7 to 1.1 dc. Physical explanations of the gains were given by analysis of the flow.
- A multi-point optimization based on three operating conditions for $M = 0.83$, $C_L \in (0.3, 0.4, 0.5)$ gave an average improvement of total drag by 1 dc, and overall a much better polar than the single-point optimization.
- Both optimums perform better than the baseline geometry.
- The drag decreases can be considered as small (~ 1 dc) compared to gains usually obtained in wing optimization problems, but the pylon has a much lower influence on the drag than a wing so a much lower potential gain; and this is equivalent to roughly a reduction 350 kg of primary mass in terms of fuel burn.
- The trade-off on the engine position with local optimization shows that the best

polars are obtained for forward engines displacements of -100 mm and -250 mm. For the dX displacement values of -50 mm and -300 mm, important flow separations appear around specific C_L ranges, which lead to large drag increase (up to 1 dc for $dX = -50$ mm and $C_L = 0.33$).

The next step will be to realize the coupling with the OAD tool in order to minimize the overall performance criteria instead of the drag - with respect to aerodynamic design variables, and so to be in position to fully implement the bi-level MDO formulation.

Acknowledgments

The studies presented in this article is making use of the elsA-ONERA software, whose the co-owners are Airbus, Safran, and ONERA.

This work is part of the MDA-MDO project of the French Institute of Technology IRT Saint Exupéry. We wish to acknowledge the PIA framework (CGI, ANR) and the project industrial members for their support, financial backing and/or own knowledge: Airbus, Altran Technologies, SOGETI High Tech, CERFACS. In particular, we warmly thank Cyril Bonnaud and Benoît Parcelier from Airbus for the discussions about pylon design.

References

[1] L. Cambier, S. Heib, and S. Plot. *The Onera elsA CFD software: input from research and feedback from industry. Mechanics & Industry*, 14(3):159–174, 2013.

[2] R. P. Dwight and J. Brézillon. *Effect of approximations of the discrete adjoint on gradient-based optimization. AIAA journal*, 44(12):3022–3031, 2006.

[3] F. Gallard. *Aircraft shape optimization for mission performance.* PhD thesis, INP Toulouse, 2014.

[4] F. Gallard, B. Mohammadi, M. Montagnac, and M. Meaux. *An adaptive multipoint formulation for robust parametric optimization. Journal of Optimization Theory and Applications*, 167(2):693–715, 2015.

[5] F. Gallard, C. Vanaret, D. Guénot, et al. *GEMS: A Python Library for Automation of Multidisciplinary Design Optimization Process Generation.* AIAA SciTech Forum. American Institute of Aeronautics and Astronautics, Jan 2018.

[6] A. Gazaix, F. Gallard, V. Gachelin, et al. *Towards the Industrialization of New MDO Methodologies and Tools for Aircraft Design.* AIAA AVIATION Forum. American Institute of Aeronautics and Astronautics, Jun 2017.

[7] M. Meaux, M. Cormery, and G. Voizard. *Viscous Aerodynamic Shape Optimization Based on the Discrete adjoint state for 3D Industrial Configurations.* ECCOMAS, 2004.

[8] L. Piegl and W. Tiller. *The NURBS Book.* Springer-Verlag, London, UK, 1997.